



# Reactivity of $C_3S$ and model cement in presence of $Na_2S_2O_3$ and NaSCN

L. Gonzalez-Panicello · A. G. De la Torre · M. Palacios 

Received: 11 August 2022 / Accepted: 10 January 2023 / Published online: 27 January 2023  
© The Author(s) 2023

**Abstract** The impact of NaSCN and  $Na_2S_2O_3$  on the reactivity, microstructure and morphology of  $C_3S$  and model cement (with a clinker containing 85%  $C_3S$  and 15%  $C_3A$ ) pastes was systematically investigated. Results concluded that both alkali salts mainly act enhancing the reactivity of the  $C_3S$  phase while not significant influence on the reactivity of  $C_3A$  was measured. While both admixtures rose the reactivity of  $C_3S$  over the studied 7 days of hydration, they only increased the reactivity of model cement pastes up to 14–20 h. NaSCN and  $Na_2S_2O_3$  did not modify the C–S–H stoichiometry but they influenced its morphology. In particular, thicker convergent C–S–H needles were formed in pastes containing  $Na_2S_2O_3$  compared to non-admixed systems, while a higher number of thinner C–S–H needles were formed in presence of NaSCN. Furthermore, greater portlandite clusters and intermixing of AFm and C–S–H were observed in

admixed  $C_3S$  and model cement pastes, respectively, compared to plain systems.

**Keywords**  $C_3S$  · Model cement · Hydration · Accelerating admixtures · Microstructure

## 1 Introduction

Accelerating admixtures are widely used chemicals to enhance the reactivity of cementitious materials [1]. Their addition to concrete formulations enables to shorten the hardening time of precast concrete, the production of ready-mix concrete at low temperatures and a fast setting for shotcrete. Furthermore, accelerating admixtures have become nowadays essential, to increase the early reactivity and mechanical performance of modern sustainable concrete with a high replacement of clinker by supplementary cementitious materials (SCMs) [2–6].

$CaCl_2$  is the most effective and widely studied accelerator for Portland cementitious systems [7, 8]. Juenger et al. [9] concluded from soft X-ray transmission microscopy, that  $CaCl_2$  accelerated the reactivity of  $C_3S$  forming a less dense C–S–H with respect to non-admixed sample that favoured the diffusion of ions and water to the  $C_3S$  particle and its further reactivity. Despite the efficiency of  $CaCl_2$  as an

---

**Supplementary Information** The online version contains supplementary material available at <https://doi.org/10.1617/s11527-023-02105-z>.

---

L. Gonzalez-Panicello · M. Palacios (✉)  
Eduardo Torroja Institute for Construction Science  
(IETcc-CSIC), Serrano Galvache 4, 28033 Madrid, Spain  
e-mail: marta.palacios@ietcc.esic.es

A. G. De la Torre  
Departamento de Química Inorgánica, Cristalografía Y  
Mineralogía, Universidad de Málaga, Facultad de  
Ciencias, Campus Teatinos, 29010 Málaga, Spain



accelerator, its dosage is limited in reinforced concrete to reduce the risk of steel corrosion.

Alkali salts such as NaOH and Na<sub>2</sub>SO<sub>4</sub> have also been shown to increase the early reactivity of alite and Portland cement [10, 11]. Kumar et al. [12] reported that the increase of the pH of the solution promoted the faster precipitation of portlandite that enhanced the undersaturation of the C<sub>3</sub>S and increased the reaction rate of alite. However, alkalis may have a negative impact on mechanical properties of cement mortars after 1–3 days [11, 12] that it is directly related to the phase assemblage of the admixed mortars and their capillary porosity. At equal alkali concentration and degree of hydration, Mota et al. [11] reported that Na<sub>2</sub>SO<sub>4</sub> lead to similar compressive strengths as for alkali-free-mortars, whereas NaOH decreased 25–35% up to 90 days. These authors showed that the addition of 0.725 M Na<sub>2</sub>SO<sub>4</sub> solution to white Portland cement favoured the formation of ettringite and a decrease of porosity with respect to non-admixed cement [11], while NaOH inhibited the formation of ettringite and increased the porosity. Furthermore, Na<sub>2</sub>SO<sub>4</sub> led to a divergent C–S–H morphology (needles do not merge to the same point) while NaOH promoted a more planar C–S–H, but these changes did not affect the mechanical strength.

Other soluble inorganic salts such as thiocyanates or thiosulfates are commonly used effective accelerators, however, very few systematic studies on their influence on the reactivity and microstructure of cementitious materials has been reported and their working mechanisms still remain unknown [13–15]. Abdelrazig et al. [13] reported that the addition of 1 wt% NaSCN to Portland cement did not modify the extension of the induction period but it enhanced the intensity of the main peak in the calorimetry curve and the reactivity of C<sub>3</sub>S after 6 h of hydration. The addition of 0.2 wt% NaSCN to OPC-fly ash blends enhanced more significantly the reactivity of the C<sub>3</sub>S than the aluminate phases and increased around 15% and 5% the mechanical strength after 2 and 28 days of curing at 20 °C, respectively [4].

Understanding which mineralogical phases of Portland cement the accelerating admixtures act on involves a great difficulty due to the complex composition of the material and the simultaneous reactions that take place. For this reason, in this paper the effect of two widely used accelerating admixtures, namely sodium thiosulfate (Na<sub>2</sub>S<sub>2</sub>O<sub>3</sub>) and sodium thiocyanate

(NaSCN) on the reactivity and microstructure of model cementitious materials that contain the most relevant mineralogical phases of cement, C<sub>3</sub>S and C<sub>3</sub>A were examined. By determining which admixtures acts on which mineral phase and at what speed more knowledge-based design of admixtures could be envisaged, something of great importance for enhancing the early mechanical performance of low clinker concrete.

## 2 Materials and methods

### 2.1 Synthesis of C<sub>3</sub>S and model cement

Pure tricalcium silicate (C<sub>3</sub>S) was synthesized by homogenizing the stoichiometric quantities of CaCO<sub>3</sub> (Calcium carbonate, reagent grade, Scharlau) and SiO<sub>2</sub> (Silica gel, Merck KGaA) in ethanol. After evaporation of the ethanol, 5 g pellets were pressed and heated at 1500 °C in platinum crucibles for 16 h. The sample was afterwards quickly quenched at room temperature in air. Samples were ground and the thermal treatment was repeated a second time.

A model clinker containing 85 wt% of C<sub>3</sub>S and 15 wt% of C<sub>3</sub>A (model clinker) was synthesized by using a similar procedure as described by Marchon et al. [16]. SiO<sub>2</sub>, CaCO<sub>3</sub>, Al<sub>2</sub>O<sub>3</sub> (Aluminium oxide anhydrous, Merck KGaA) and MgO (Magnesium oxide 90%, Panreac) in a molar ratio of 1:2.23:0.198:0.058 were homogenized in ethanol for 1 h. After the evaporation of the ethanol, 5 g pellets were pressed and treated at 1500 °C for 16 h in platinum crucibles. Samples were quickly quenched in air afterwards.

Around 50 g of C<sub>3</sub>S and model clinker samples were dry ground in a planetary ball mill (Pulverisette, Fritsch) using a 500 ml jar and agate beads and sieved

**Table 1** Mineralogical composition (wt%) of C<sub>3</sub>S and model clinker determined by Rietveld method

Sample	Mineralogical phase	wt%
C <sub>3</sub> S	Triclinic C <sub>3</sub> S (T <sub>1</sub> )	> 99.5 (3)
	Lime	< 0.5 (3)
Model clinker	Monoclinic C <sub>3</sub> S (M <sub>3</sub> + M <sub>1</sub> )	84.3 (3)
	Cubic C <sub>3</sub> A	15.1 (3)
	Lime	0.6 (3)



afterwards through a 45  $\mu\text{m}$  mesh. Table 1 shows the mineralogical composition of both synthetic phases determined by the Rietveld analysis of the XRD patterns (see Figure S1 of Supplementary material). The particle size distribution (see Fig. 1) was measured by laser diffraction (MALVERN MASTERSIZER S) using isopropanol as dispersant and the optical model parameters described in [17]. Table 2 shows the characteristic particle diameters (volume based) of the synthetic phases and Fig. 1 the particle size distribution. Table 2 also shows the specific surface area ( $\text{SSA}_{\text{BET}}$ ) of  $\text{C}_3\text{S}$  and the model clinker determined by using a BET multi-point nitrogen adsorption equipment (ASAP 2010-Micromeritics). The samples were previously degassed at 200  $^\circ\text{C}$  during 2 h under vacuum [17].

Calcium sulfate hemihydrate was used as the sulfate carrier for the model clinker and it was obtained by thermal treatment of gypsum (98% pure, Acros Organics) at 110  $^\circ\text{C}$  for 16 h. Gypsum was previously sieved < 20  $\mu\text{m}$ . Model clinker was mixed by hand for 10 min in an agate mortar with 5.5% (w/w) of calcium sulfate hemihydrate [18] that ensured the suitable sulphated level for the model cement

according to the calorimetry curve shown in Figure S2 in the supplementary material.

## 2.2 Preparation of pastes

$\text{C}_3\text{S}$  and model cement pastes were prepared at a liquid/solid ratio of 0.35 and 0.4, respectively. 10 g of solid were mixed with ultrapure water (18.2  $\text{M}\Omega\cdot\text{cm}$  by a Milli-Q A + water purification system from Millipore, Merck & Cie) at 200 rpm for 30 s and 800 rpm for 3 min with a 2-bladed propeller stirrer (JANKE KUNKEL IKA-WERK RW 20). 0.3wt% of NaSCN (NaSCN 8 M from Sigma Life Science) and 0.3 wt% and 2 wt% of  $\text{Na}_2\text{S}_2\text{O}_3$  (99% purity from Acros Organics) by weight of powder (bwp) was added into the mixing water. These dosages previously showed to effectively accelerate the reactivity of Portland cement pastes by isothermal calorimetry (see Figure S3 in the supplementary material).

## 2.3 Hydration kinetics

The hydration kinetics were determined using an isothermal calorimeter TAM Air (TA Instruments) set

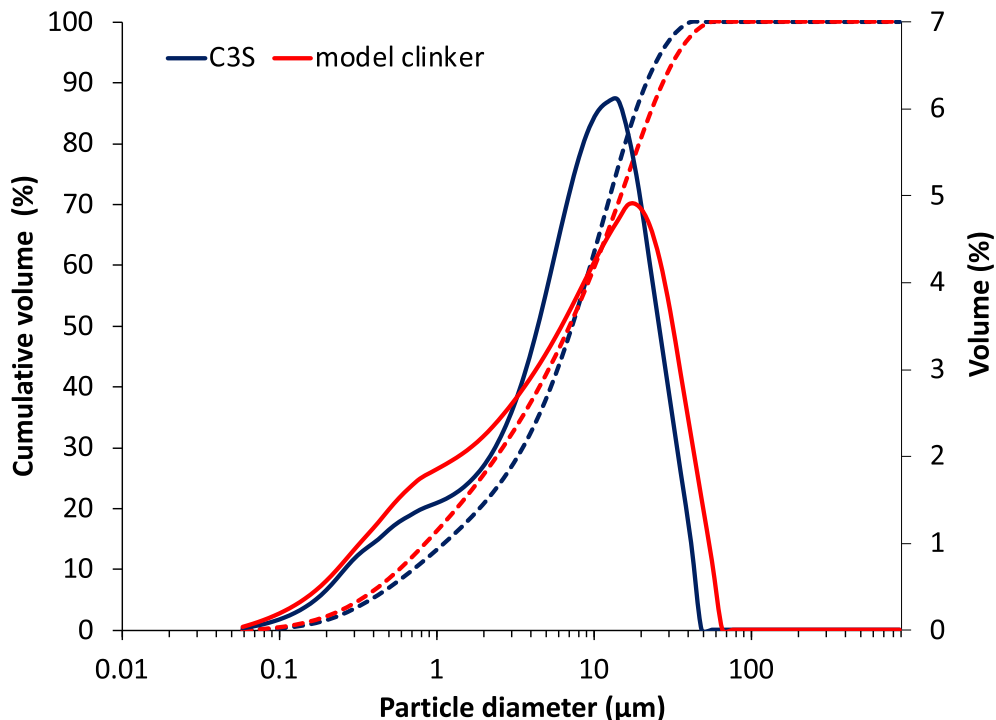


**Fig. 1** Particle size distribution of  $\text{C}_3\text{S}$  and model clinker

**Table 2** Particle size distribution and specific surface area of C<sub>3</sub>S and model clinker

Sample	SSA (m <sup>2</sup> /g)	Dv <sub>10</sub> (μm)	Dv <sub>50</sub> (μm)	Dv <sub>90</sub> (μm)
C <sub>3</sub> S	0.9	0.7	7.3	21.6
Model Clinker	1.3	0.6	7.0	31.1

at 25 °C. 5 g of the pastes was introduced into the calorimeter. The measurement during the first 30 min were not considered as this is the time required for the equipment to stabilize the temperature after introducing the sample. An enthalpy of hydration of C<sub>3</sub>S and C<sub>3</sub>A of 517 J/g [19] and 1340 J/g [20], respectively, were used to calculate the degree of reaction of the C<sub>3</sub>S and the model cement.

#### 2.4 Mineralogical characterization of the solids

The hydration of C<sub>3</sub>S and model cement pastes was stopped after 8 h, 1, 2 and 7 days of reaction by mixing with isopropanol (1 g of paste + 10 g of isopropanol) for 1 min. The suspension was filtered afterwards through a nylon filter with a pore size of 0.45 μm and the powder was kept in a desiccator at low vacuum (700 mbar) to avoid ettringite dehydration [21].

Phase identification including Rietveld quantitative analysis was carried out on data collected with a X'Pert PRO MPD (PANalytical) diffractometer (located at SCAI of University of Malaga) in a  $\Theta$ -2 $\Theta$  configuration using a CuK $\alpha_1$  (1.5406 Å) radiation (monochromatized with a primary Ge (1 1 1) monochromator). The samples were scanned between 5° and 70°, with a step size 0.0167° and with a detection system that consists of a X'Celerator RTMS (Real Time Multiple Strip) constituted by 128 Si detectors. The internal standard method was applied to quantify the phase content using quartz (Silicon (IV) oxide, 99.5%, Alfa Aesar) as a standard according to the methodology proposed in the literature [22].

Rietveld Analyses were performed with TOPAS software (Bruker). The overall refined parameters were: phase fractions, zero of goniometer, unit cell, crystal size and strain (in C<sub>3</sub>S) and preferred orientation when appropriated. The Brindley microabsorption correction [23] was applied to the anhydrous and stopped pastes with internal standard by a post-analysis mathematical treatment.

Thermogravimetric analysis (TGA) of the pastes at different hydration times was carried out by using a TGA-DCS-DTA Q600 (TA instruments) equipment. Around 40 mg of sample in an alumina (Al<sub>2</sub>O<sub>3</sub>) crucible was heated from 25 up to 1000 °C with a rate of 10 °C/min under a 100 ml/min flow of N<sub>2</sub>. Bounded water, portlandite and calcite content were calculated according to [24]. These data were used in conjunction with the quantitative Rietveld analysis of the XRD patterns to determine the phase assemblage of the pastes as a function of time [22, 25].

#### 2.5 Morphological and microstructural characterization of the pastes

C<sub>3</sub>S and model cement pastes, with and without admixtures, were prepared according to Sect. 2.2, cast in 1 × 1 × 0.5 cm<sup>3</sup> moulds and cured during 7 days at 25 °C and 99% RH. Afterwards the samples were submerged in isopropanol for 5 days to stop the hydration and subsequently kept in a desiccator until constant weight.

The microstructure was analyzed by backscattered scanning electron microscopy using a Hitachi S-4800 microscope. Energy dispersive X-ray (EDX) measurements were done with an Oxford Instruments X-Max detector. Hydrated samples at 7 days were previously embedded in epoxy resin, polished and carbon coated.

The surface of hydrated C<sub>3</sub>S samples with and without admixtures, at a degree of reaction of 9% (according to the calorimetry curves), was studied by scanning electron microscopy (SEM) using a JEOL JSM 7600F microscope. The hydration was previously stopped with isopropanol as explained in Sect. 2.4. The dried powder was dispersed on an adhesive carbon tab and coated with a chromium film using a modular coating system for the deposition of electrically conductive films (Quorum Q150T E).

The specific surface area of hydrated C<sub>3</sub>S samples (with a DoR = 9%) were measured by using a BET



multi-point nitrogen physisorption device (Micromeritics Tristar II Plus, Micromeritics). The samples previously were degassed at 40 °C for 16 h in N<sub>2</sub> flow [26] by a VacPrep 061 LB sample degassing system from Micromeritics.

### 3 Results

#### 3.1 Hydration kinetics

Figure 2 shows the evolution of the heat flow and cumulative heat of C<sub>3</sub>S and model cement pastes, with and without admixtures. In admixture-free pastes (Fig. 2a, b, black lines), a delay of the time of appearance of the peak assigned to the silicates hydration is observed in model cement pastes with respect to C<sub>3</sub>S pastes. This can be explained by the well-known retardation induced by the aluminates

released by the aluminium-doped alites (monoclinic polymorphism) that are not present in pure C<sub>3</sub>S (triclinic polymorphism) [27, 28].

In C<sub>3</sub>S pastes (Fig. 2a), the addition of NaSCN and Na<sub>2</sub>S<sub>2</sub>O<sub>3</sub> reduces the time of appearance of the main peak in the calorimetry curve and enhances the slope of the acceleration period with respect to the admixture-free paste. At equal dosages, 0.3 wt% of NaSCN and Na<sub>2</sub>S<sub>2</sub>O<sub>3</sub> in C<sub>3</sub>S pastes induce a similar acceleration of around 30 min with respect the plain sample. An increase of the dosage of Na<sub>2</sub>S<sub>2</sub>O<sub>3</sub> up to 2 wt% accelerated its appearance by 1 h and doubled the intensity of the main peak from 5 mW/g C<sub>3</sub>S to 10 mW/g C<sub>3</sub>S. Both, Na<sub>2</sub>S<sub>2</sub>O<sub>3</sub> and NaSCN enhanced the cumulative heat of C<sub>3</sub>S over the 7 days as shown in Fig. 2b. At 8 h of hydration, the addition of 2 wt% Na<sub>2</sub>S<sub>2</sub>O<sub>3</sub> led to the highest values of cumulative heat (with an increase of around 62% with respect to non-admixed C<sub>3</sub>S) while at 7 days of hydration, both,

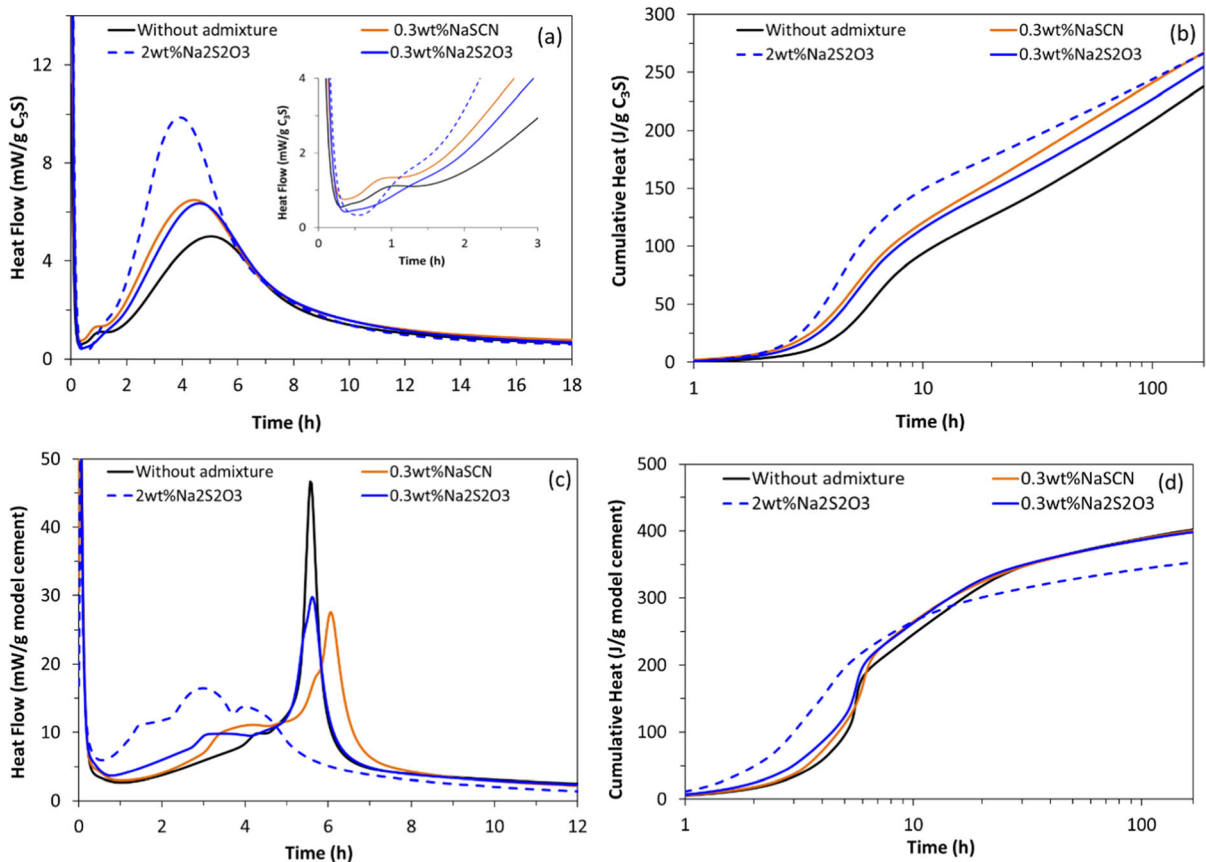


**Fig. 2** Heat flow and cumulative heat of **a, b** C<sub>3</sub>S and **c, d** model cement pastes in absence and presence of 0.3 wt% NaSCN and 0.3 wt% and 2 wt% Na<sub>2</sub>S<sub>2</sub>O<sub>3</sub>

0.3 wt% NaSCN and 2 wt% Na<sub>2</sub>S<sub>2</sub>O<sub>3</sub> enhanced up to 12% of the cumulative heat with respect to the plain C<sub>3</sub>S.

The acceleration of the C<sub>3</sub>S reactivity by alkalis have been previously explained by the promotion of portlandite precipitation with the increase of the pH of the solution that reduces the amount of Ca<sup>2+</sup> in solution, increases the level of C<sub>3</sub>S undersaturation and consequently enhances its dissolution [3, 12]. When we look in further detail the heat flow evolution of the C<sub>3</sub>S pastes over the first 3 h, a slight acceleration of the time of appearance and the intensity of the first shoulder normally assigned to the initial portlandite precipitation is observed in presence of 0.3 wt% NaSCN with respect to plain C<sub>3</sub>S as previously reported for KOH and NaOH in alite pastes [12]. In contrast, the addition of Na<sub>2</sub>S<sub>2</sub>O<sub>3</sub> delayed the time of appearance of this shoulder with respect to the free-admixtures sample. Similar extension of the induction period has been observed in alite samples containing gypsum [29]. To understand the impact of both alkali salts on portlandite precipitation, a further analysis was done by TGA and is discussed in Sect. 3.2.

In the model cement pastes (Fig. 2c, d), the addition of 0.3 wt% of NaSCN accelerated by 1 h the time of appearance of the main peak associated mainly to the silicate hydration (observed at around 3.5 h) while it delayed and decreased the intensity of the second peak associated with the renewed hydration of C<sub>3</sub>A after sulphate depletion [21]. 0.3 wt% of Na<sub>2</sub>S<sub>2</sub>O<sub>3</sub> did not affect the position and intensity of the aluminates peak, while it accelerated by 1 h the time of appearance of the silicates peak. At dosages of 2 wt% of Na<sub>2</sub>S<sub>2</sub>O<sub>3</sub>, a broad peak is observed and silicates and aluminates hydration peaks cannot be clearly distinguished that infers that the reactions of C<sub>3</sub>S and C<sub>3</sub>A are very close in time. Similar effect has been reported in the literature when NaOH or Na<sub>2</sub>SO<sub>4</sub> were used as accelerators in cement systems [5, 11]. Both, NaSCN and Na<sub>2</sub>S<sub>2</sub>O<sub>3</sub> had a positive impact on the cumulative heat of the model cement over the first 14 h, while afterwards the addition of 2 wt% Na<sub>2</sub>S<sub>2</sub>O<sub>3</sub> reduced the cumulative heat with respect plain model cement pastes.

### 3.2 Chemically bounded water and phase assemblage

#### 3.2.1 Thermogravimetry analysis

An increase of the amount of chemically bounded water in plain and admixed pastes was measured with the increase of the hydration time as shown in Fig. 3. This increase in chemically bounded water obtained by TGA (Figures S4 and S5 in the Supplementary Material), and heat released followed a linear trend for all pastes studied as shown in the Figure S6 in the Supplementary Material.

In C<sub>3</sub>S pastes, the addition of 2 wt% Na<sub>2</sub>S<sub>2</sub>O<sub>3</sub> and 0.3 wt% NaSCN led to the highest values of bounded water compared to plain pastes that infers the highest formed amount of hydration products. In particular, the addition of 2 wt% Na<sub>2</sub>S<sub>2</sub>O<sub>3</sub> increased, respectively, 19% and 5% the amount of bounded water at 2 and 7 days of hydration. Moreover, 0.3 wt% NaSCN increased around 6–14% the amount of bounded water at all the studied ages. At 7 days of hydration, C<sub>3</sub>S pastes containing 0.3 wt% NaSCN and 2 wt% Na<sub>2</sub>S<sub>2</sub>O<sub>3</sub> had similar values of bounded water contents. The effect of these admixtures on the bounded water in model cement pastes was less marked. While the presence of 0.3 wt% Na<sub>2</sub>S<sub>2</sub>O<sub>3</sub> and NaSCN increased around 1.5–2.5% the bounded water with respect the plain pastes, a decrease of around 3.5% was observed with 2 wt% Na<sub>2</sub>S<sub>2</sub>O<sub>3</sub> after 7 days of reaction. This reduction of the amount of chemically bounded water of the model cement in presence of 2 wt% Na<sub>2</sub>S<sub>2</sub>O<sub>3</sub> agrees with the reduction of the cumulative heat measured by isothermal calorimetry shown in Fig. 2d.

The amount of portlandite with respect to the anhydrous C<sub>3</sub>S and model cement was calculated according to Eq. 1, considering the weight loss between 25 and 550 °C measured by TGA [24]:

$$\begin{aligned} \text{Ca(OH)}_2, \text{ dry} &= \frac{\text{Ca(OH)}_2, \text{ measured}}{1 - \text{H}_2\text{O bounded}} \\ &= \frac{\text{WL Ca(OH)}_2}{\text{PM}_{\text{H}_2\text{O}} - \text{H}_2\text{O bounded}} \text{PM}_{\text{Ca(OH)}_2} / 1 \end{aligned} \quad (1)$$

where WL<sub>Ca(OH)<sub>2</sub></sub> is the water loss due to portlandite decomposition (in percentage); PM<sub>H<sub>2</sub>O</sub> is the molecular mass of water, PM<sub>Ca(OH)<sub>2</sub></sub> is the molecular mass of portlandite and H<sub>2</sub>O bounded is the amount of bounded water (in percentage) shown in Fig. 3.



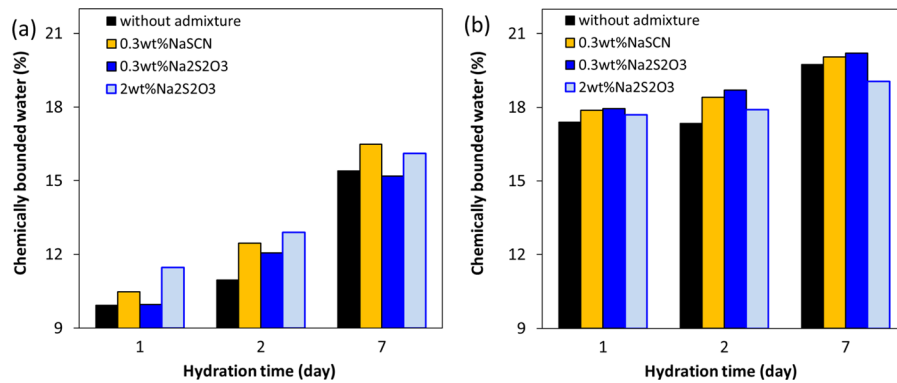


**Fig. 3** Percentage of bounded water at 1, 2 and 7 days of hydration of **a** C<sub>3</sub>S (the amount of carbonated portlandite was considered in the calculation) and **b** model cement pastes

The presence of both accelerating admixtures enhanced the amount of portlandite formed in C<sub>3</sub>S pastes from the first day of hydration as shown in Fig. 4. In particular, the addition of 2 wt% Na<sub>2</sub>S<sub>2</sub>O<sub>3</sub> led to the highest amount of portlandite at 1 day of hydration, with an increase of up to 30% with respect to non-admixed C<sub>3</sub>S pastes. In model cement pastes, the presence of 0.3 wt% of both alkali salts did not have a significant impact on the amount of portlandite formed, while 2 wt% Na<sub>2</sub>S<sub>2</sub>O<sub>3</sub> decreased up to 5–10% the portlandite content over the 7 days of hydration. The linear correlation between the portlandite content and the degree of hydration calculated from calorimetry (see Fig. 5) concludes that the impact of both accelerating admixtures on the amount of portlandite is a consequence of its effect on the reactivity of the pastes. This suggests that both alkali salts enhanced the degree of hydration of C<sub>3</sub>S and consequently also the amount of portlandite formed, while the decrease

of portlandite induced by 2 wt% Na<sub>2</sub>S<sub>2</sub>O<sub>3</sub> in model cements is due to the slowdown of its reaction after 14 h in agreement with the results obtained by calorimetry (see Fig. 2b).

### 3.2.2 Quantitative X-ray powder diffraction analysis

Rietveld quantitative phase analysis (RQPA) of the XRD patterns of non-admixed and admixed C<sub>3</sub>S and model cement pastes were done to establish the impact of the accelerating admixtures on the phase assemblages (type and amount of hydration products). It is worth highlighting that the starting C<sub>3</sub>S had around 10 wt% of amorphous fraction that might be due to its amorphisation during the dry-grinding process [30] but also to the partial prehydration of the sample as shown by the presence of Q<sup>o</sup> hydroxylated Si units in the {<sup>1</sup>H} <sup>29</sup>Si CPMAS NMR [19] in Figure S7 in the Supplementary Material. The same arguments would

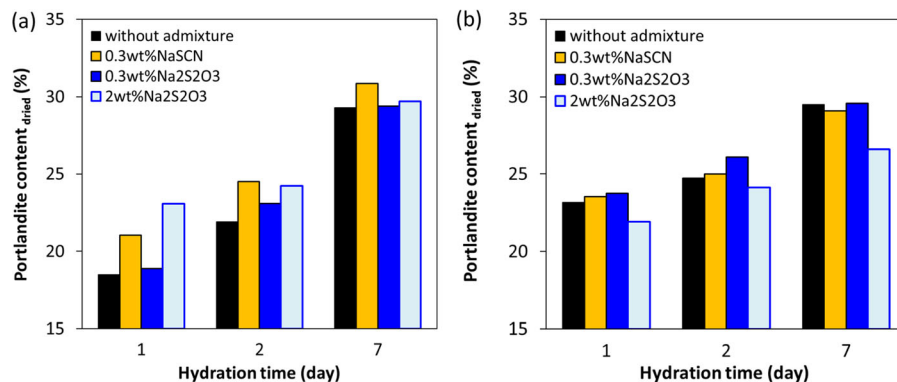


**Fig. 4** Portlandite content measured by TGA of **a** C<sub>3</sub>S (considering the contribution of carbonated portlandite) and **b** model cement pastes over hydration time

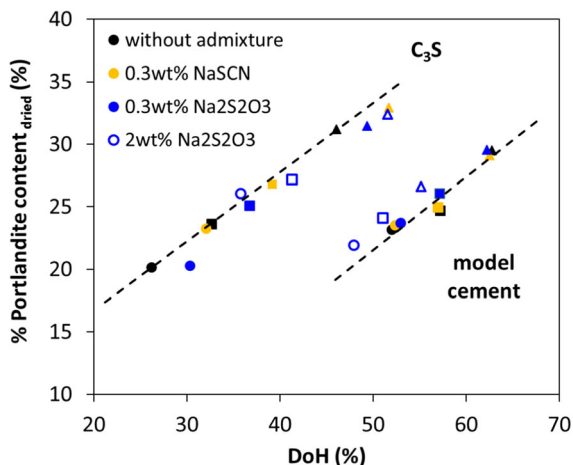


**Fig. 5** Portlandite content measured by TGA (%) versus degree of hydration measured by isothermal calorimetry (%) for  $C_3S$  and model cement pastes in presence of the alkali salts at 1 day (circle), 2 days (square) and 7 days (triangle) of hydration. (In  $C_3S$  pastes, the possible carbonation of the portlandite has been considered in the calculations)

explain the 11 wt% of amorphous phase determined in the starting model clinker. In hydrated  $C_3S$  pastes, the quantified amount of amorphous content corresponds mainly to the C–S–H formed from the  $C_3S$  hydration with small contributions from non-hydrated amorphous  $C_3S$  and possible amorphous portlandite as discussed below.

Figures S8 and S9 in the Supplementary Material show the raw LXRPD patterns of all the pastes. Figures S10 and S11 give, as representative examples, the Rietveld plots of selected patterns. Tables S1 and S6 in Supplementary material give the phase assemblage, including the amorphous phase (ACn) and free water determined by TGA, of all pastes as a function of hydration time.

Figures 6, 7 and 8 present the evolution of selected crystalline and amorphous phases (ACn) in  $C_3S$  and model cement pastes over time. All Rietveld analysis had a  $R_{WP}$  lower than 10% that confirms good refinements. Due to differences in the linear absorption coefficients among phases [ $\sim 310 \text{ cm}^{-1}$  for  $C_3S$ ,  $\sim 270 \text{ cm}^{-1}$  for  $C_3A$ ,  $\sim 40 \text{ cm}^{-1}$  for CH and  $\sim 25 \text{ cm}^{-1}$  for AFt] and the internal standard [ $\sim 90 \text{ cm}^{-1}$  for quartz] the microabsorption effect has a relevance in the RQPA [23]. Consequently, the Brindley correction was performed in a post-refinement spreadsheet calculation. The average particle size of each phase has to be known to apply such

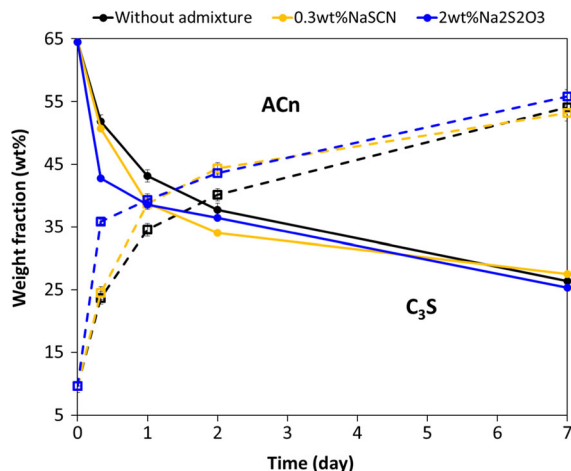


**Fig. 6** Weight percentage of  $C_3S$  and amorphous phase (ACn) in  $C_3S$  pastes without admixtures, with 0.3 wt% NaSCN and 2 wt%  $Na_2S_2O_3$  from Tables S1–S3 in the Supplementary Material

correction. For quartz, and phases in non-hydrated  $C_3S$  and model cement particle sizes were determined by laser diffraction (see Fig. 1) while for hydrated  $C_3S$  and model cement pastes, particle sizes of hydrated phases were estimated from scanning electron microscopy. In  $C_3S$  pastes, portlandite and calcite were identified as the main crystalline phases while portlandite, ettringite, calcium hemicarboaluminate and calcite were identified in the model cement pastes. In addition, calcium monosulfoaluminate was found in model cement pastes containing 0.3 wt% NaSCN. The presence of calcite and hemicarboaluminate in the samples confirm their partial carbonation due to reaction with the atmospheric  $CO_2$  during sample preparation and measurements. The quantification of portlandite by XRD is usually underestimated due to the presence nano-portlandite with a crystal size below the size of the coherent scattering domains detectable by X-rays [31]. For this reason, in this paper, we have relied on the TGA measurements for the determination of the portlandite content as already discussed in Sect. 3.2.1.

Figures 6 and 7 indicate that 2 wt%  $Na_2S_2O_3$  mainly influenced the reactivity of  $C_3S$  in pure  $C_3S$  pastes and model cement pastes while it did not modify the amount of  $C_3A$  in model cement pastes over the studied time.  $C_3S$  pastes containing 2 wt%  $Na_2S_2O_3$  showed respectively a decrease of 19% and 12% of  $C_3S$  with respect plain pastes, at 8 h and 1 day,

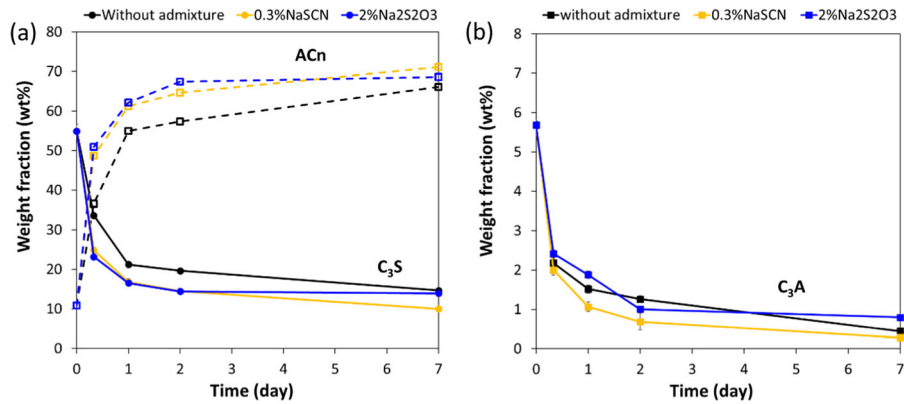


**Fig. 7** Weight percentage of **a** C<sub>3</sub>S and amorphous phase (ACn) and **b** C<sub>3</sub>A content in model cement pastes with 0.3 wt% NaSCN and 2 wt% Na<sub>2</sub>S<sub>2</sub>O<sub>3</sub> from Tables S4–S6

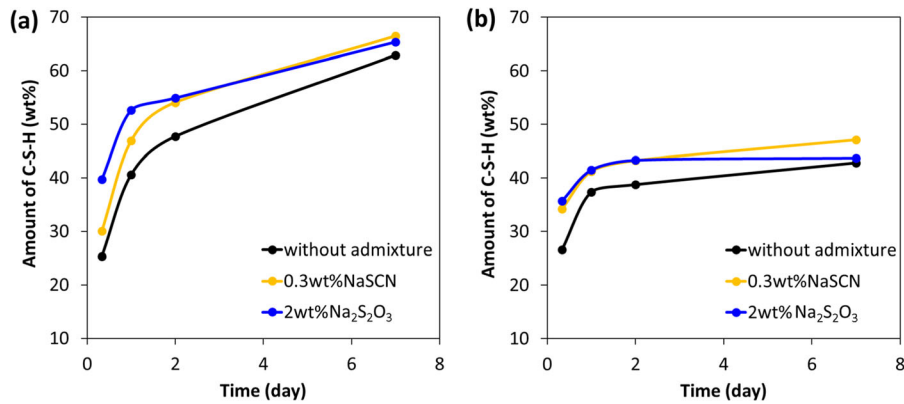


**Fig. 8** Evolution of the percentage of C–S–H obtained for the admixed **a** C<sub>3</sub>S pastes and **b** model cement pastes over hydration time

while a decrease of around 4% occurred at 2 and 7 days of hydration. After 1 day of hydration, the addition of 2 wt% Na<sub>2</sub>S<sub>2</sub>O<sub>3</sub> to model cement decreased around 17% and 24% the amount of C<sub>3</sub>S compared to non-admixed paste, after 1 day and 2 days, respectively, while it did not have impact on this phase at 7 days of hydration with respect to non-admixed paste.

The addition of 0.3 wt% NaSCN mainly enhanced the reactivity of C<sub>3</sub>S in the model cement. Around 20% more C<sub>3</sub>S reacted at 1 and 2 days of hydration but no enhancement of the reactivity was observed at 7 days of hydration, while the measured changes in the amount of C<sub>3</sub>A were small and inside the error analysis of the quantification method.

As explained above, the amorphous content determined by XRD corresponds to the remaining amorphous C<sub>3</sub>S, amorphous portlandite and C–S–H. The

amount of C–S–H was consequently calculated from the portlandite content determined by TGA (see Fig. 4) and the stoichiometry for C<sub>3</sub>S hydration shown in Eq. 2. The C<sub>1.67</sub>SH<sub>2.5</sub> stoichiometry was established by comparing the theoretical values of the C–S–H water and portlandite with the experimental values determined by TGA [32]. Considering the amount of portlandite determined by TGA after 7 days, the total reaction of the initial amorphous C<sub>3</sub>S (~ 10 wt%) has to be considered. Moreover, to estimate the amount of C–S–H formed, a stoichiometry has to be assumed. The Ca/Si rate from 1.6 to 1.8 and the water molecules of C–S–H from 2.1 to 4 were tested, to match the RQPA obtained and given in Tables S1 to S3. Finally, the determined stoichiometric was:



**Table 3** Theoretical and experimental data of weight loss from C–S–H and from CH obtained by Eq. 2 on C<sub>3</sub>S pastes without and with the presence of 0.3 wt% NaSCN and 2 wt% Na<sub>2</sub>S<sub>2</sub>O<sub>3</sub> at 7 days oh hydration

	Without admixture		0.3 wt% NaSCN		2 wt% Na <sub>2</sub> S <sub>2</sub> O <sub>3</sub>	
	Theoretical	Experimental	Theoretical	Experimental	Theoretical	Experimental
% C–S–H water	10.6	10.0	10.4	10.9	10.9	10.7
% CH water	5.7	5.4	5.6	5.3	5.8	5.4

With this stoichiometry the water losses from C–S–H and from portlandite were theoretically calculated and compared to those obtained experimentally by TGA, Table 3. From this, it was inferred that the presence of NaSCN and Na<sub>2</sub>S<sub>2</sub>O<sub>3</sub> did not largely affect to the C–S–H stoichiometry. The morphology and stoichiometry of C–S–H gels are highly dependent on the ionic environment [33], however, because of the overlapping signals assigned to the dehydration of ettringite and C–S–H in TGA, the calculation of the C–S–H stoichiometry for model cement pastes was not possible.

The evolution of the amount of C–S–H formed in C<sub>3</sub>S and model cement pastes over time is shown in Fig. 8. In C<sub>3</sub>S pastes, the presence of both alkaline salts increased the amount of C–S–H up to 7 days of hydration, being more significant with the addition of 2 wt% Na<sub>2</sub>S<sub>2</sub>O<sub>3</sub>. In contrast, while 0.3 wt% NaSCN enhances the C–S–H precipitation over the 7 days of hydration, the addition of 2 wt% Na<sub>2</sub>S<sub>2</sub>O<sub>3</sub> only increases the amount of C–S–H up to 2 days. This would confirm that Na<sub>2</sub>S<sub>2</sub>O<sub>3</sub> only rises the reactivity of model cement pastes at early ages, as already concluded from the amount of chemically bounded water (Fig. 3b) and calorimetry measurements (Fig. 2d).

### 3.3 Impact of Na<sub>2</sub>S<sub>2</sub>O<sub>3</sub> and NaSCN on the morphology and microstructure of the pastes

#### 3.3.1 Morphology of hydrates on admixed C<sub>3</sub>S pastes

Isothermal calorimetry and QXRD measurements showed the effect of Na<sub>2</sub>S<sub>2</sub>O<sub>3</sub> and NaSCN acted mainly on the reactivity of C<sub>3</sub>S. For this reason, the morphology of the reaction products on these pastes was studied at a degree of hydration (DoH) of 9%

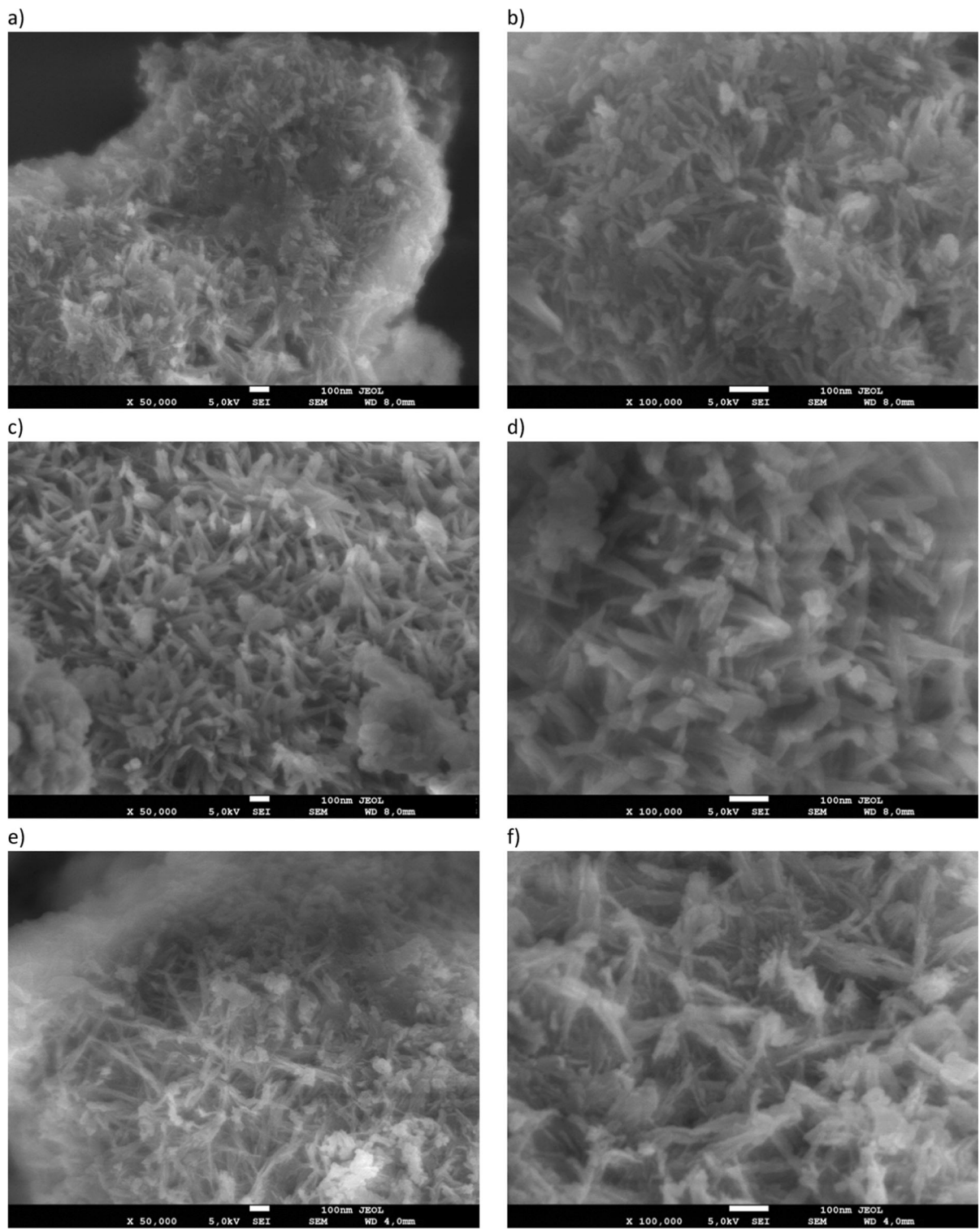
(according to the isothermal calorimetry, see Fig. 2). This degree of hydration corresponded to the acceleration period where nucleation and growth of hydrates occurred.

Figure 9 shows the surface of the plain and admixed C<sub>3</sub>S pastes covered by hydrates. C–S–H needles that grow outwards from the C<sub>3</sub>S surface and merge together to a same point were observed in all cases, however the presence of the admixtures seemed to influence the thickness of the C–S–H needles. While Na<sub>2</sub>S<sub>2</sub>O<sub>3</sub> induced the formation of slightly thicker needles, thinner C–S–H needles were formed in NaSCN-containing pastes. These results are in agreement with the SSA<sub>BET</sub> values of the pastes. In particular, SSA<sub>BET</sub> of 5.4, 4.3 and 9.9 g/m<sup>2</sup> were measured for plain, Na<sub>2</sub>S<sub>2</sub>O<sub>3</sub>- and NaSCN-C<sub>3</sub>S containing pastes, respectively.

#### 3.3.2 Microstructure and hydrates composition of C<sub>3</sub>S and model cement pastes

Figures 10 and 11 show the microstructure of C<sub>3</sub>S and model cement pastes at 7 days of hydration. For C<sub>3</sub>S pastes in absence of admixtures, thin dense C–S–H rims (inner product) are observed around the C<sub>3</sub>S particles while outer C–S–H product with a greater porosity is formed in the initially water-filled space exterior to the original C<sub>3</sub>S grains. In contrast, the thickness of the inner-C–S–H rims is significantly reduced in C<sub>3</sub>S pastes containing both alkali salts, and outer C–S–H is mainly observed. Furthermore, NaSCN-containing C<sub>3</sub>S pastes showed a much greater porosity (black contrast) than the plain samples. The addition of both alkali salts also led to the formation of portlandite clusters. EDX analyses of the matrices (see Table 4) indicate a higher Ca/Si ratio for the admixed C<sub>3</sub>S pastes that would infer that the admixtures favour the intermixing of C–S–H and portlandite as it was





**Fig. 9** SEM images of the surface of  $C_3S$  pastes at 9% degree of hydration, **a, b** plain  $C_3S$  and  $C_3S$  with **c, d** 2 wt%  $Na_2S_2O_3$  and **e, f** 0.3 wt%  $NaSCN$

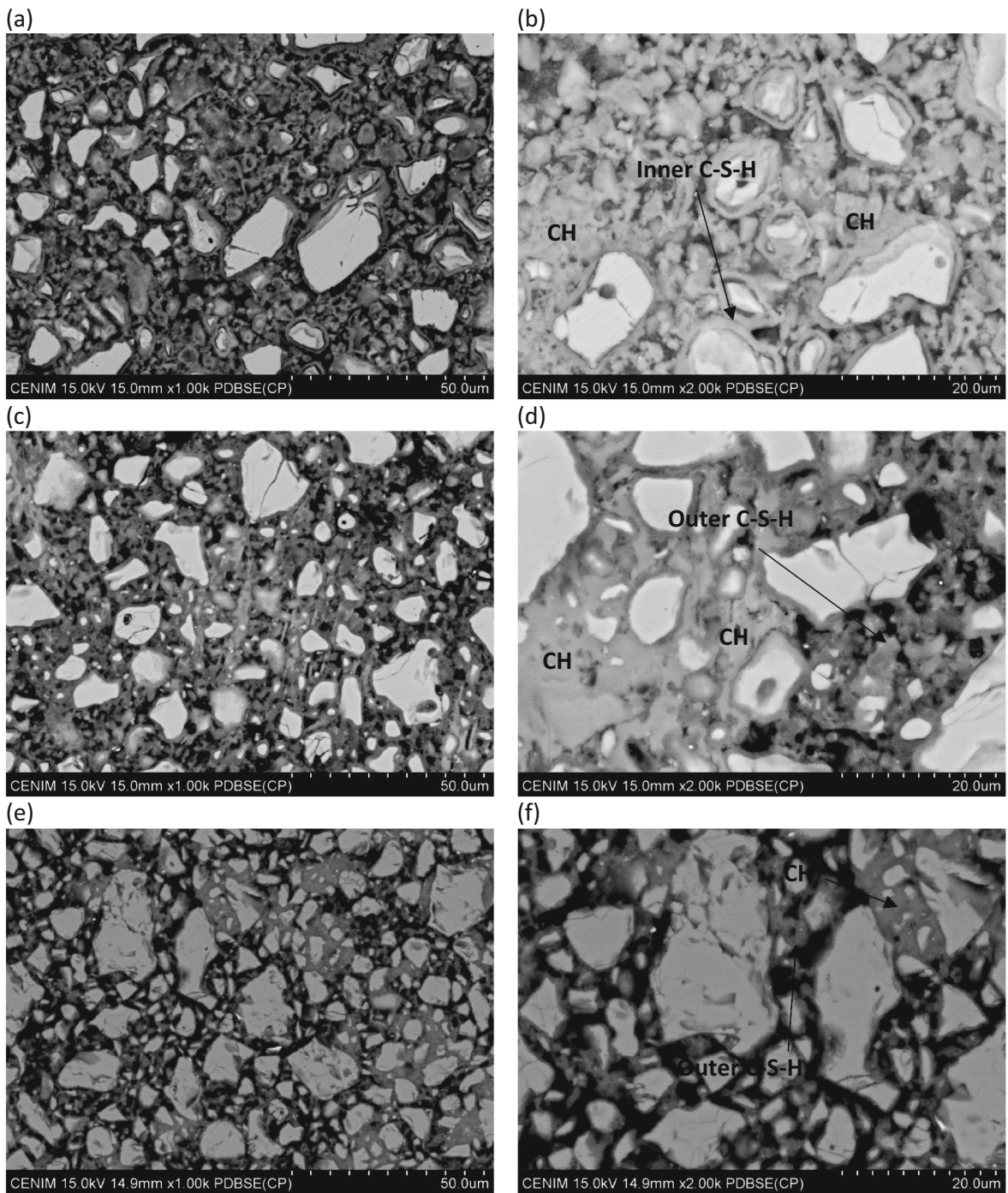


**Fig. 10** BSE micrographs of  $C_3S$  pastes after 7 days of hydration **a, b** without admixture, **c, d** 2 wt%  $\text{Na}_2\text{S}_2\text{O}_3$  and **e, f** 0.3 wt%  $\text{NaSCN}$

determined that they did not modify the C–S–H stoichiometry as previously described in Sect. 3.2.2.

In the model cement pastes, the addition of  $\text{NaSCN}$  tended to decrease the density of the matrix and no C–

S–H ring around the anhydrous particles was observed. The addition of both alkali salts led to the precipitation of AFm phases intermixed with the outer C–S–H as it can be also observed in the two

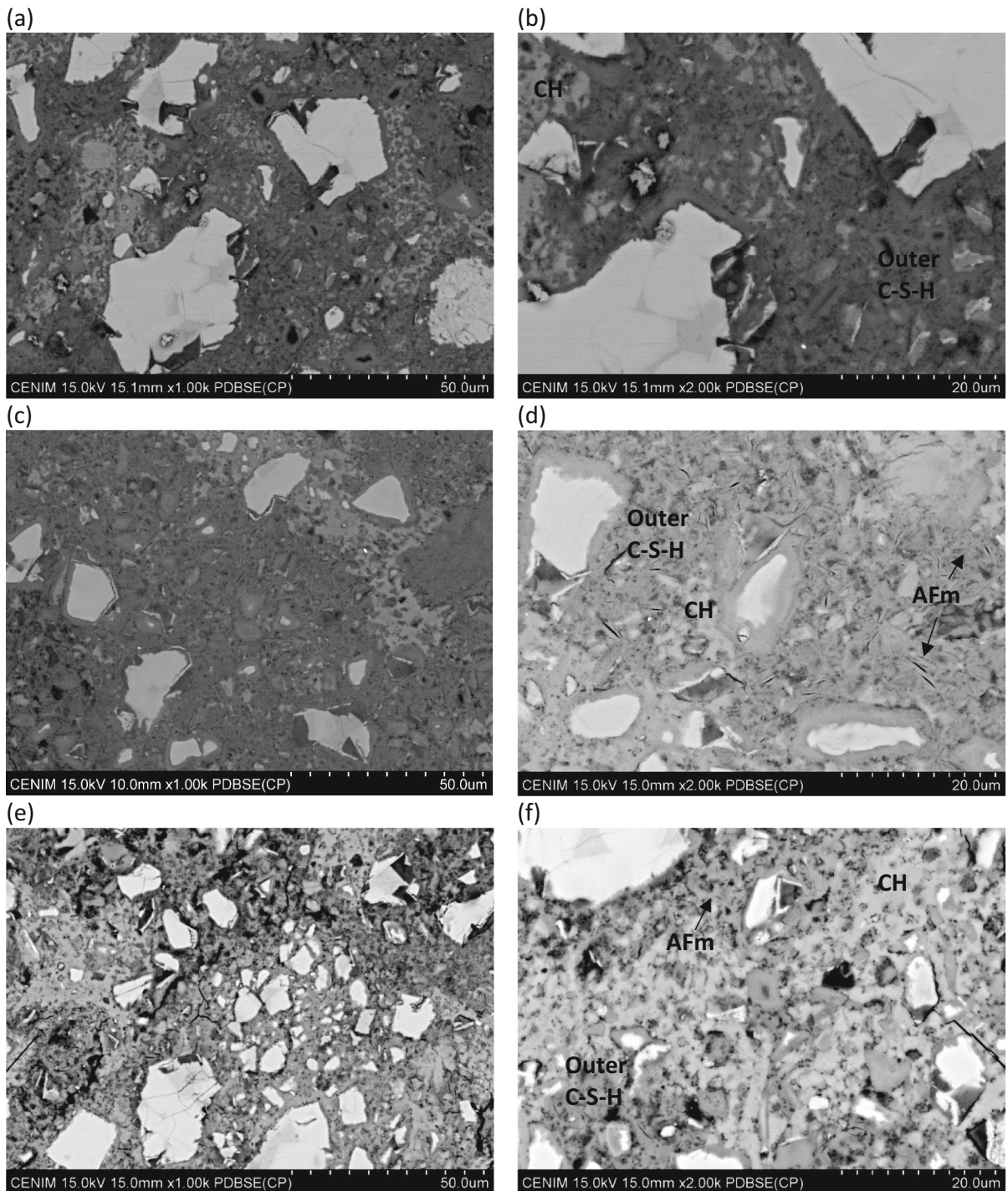


**Fig. 11** BSE micrographs of model cement pastes after 7 days of hydration **a, b** without admixture, **c, d** 2 wt% Na<sub>2</sub>S<sub>2</sub>O<sub>3</sub> and **e, f** 0.3 wt% NaSCN

dimensional scatter plots of atomic ratio (see Fig. 12) [34, 35]. From the BSEM analysis, more AFm seems

to be formed in Na<sub>2</sub>S<sub>2</sub>O<sub>3</sub>-containing samples with respect to model cement pastes with NaSCN. The

**Table 4** EDX analyses of the matrices in  $C_3S$  pastes at 7 days of hydration

Sample	Ca/Si ratio
$C_3S$ without admixture	$1.72 \pm 0.40$
$C_3S + 2 \text{ wt\% } Na_2S_2O_3$	$2.27 \pm 0.41$
$C_3S + 0.3 \text{ wt\% } NaSCN$	$2.09 \pm 0.48$

presence of NaSCN and  $Na_2S_2O_3$  also lead to the formation of large portlandite clusters, as already described for  $C_3S$  pastes (see Fig. 11).

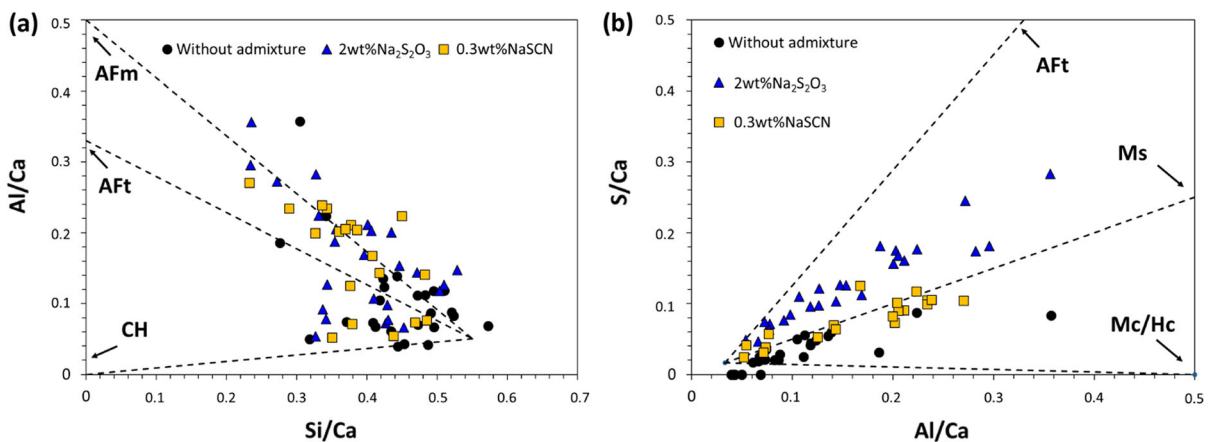
#### 4 Discussion

The discussion of our results has been divided in two main sections. In the first one, the impact of NaSCN and  $Na_2S_2O_3$  on the reactivity and hydrates formation in the main cement phases is discussed based on the isothermal calorimetry, QXRD and TGA results, while the second part focuses on the morphology and microstructure of the admixed pastes.

##### a. Influence of NaSCN and $Na_2S_2O_3$ on the reactivity

Hydration kinetics measurements have shown the faster reactivity of  $C_3S$  and model cement (compound of a model clinker (85 wt%  $C_3S$ , 15 wt%  $C_3A$ ) and 5.5%w/w calcium hemihydrate) in presence of 0.3 wt% NaSCN and 0.3–2 wt%  $Na_2S_2O_3$ . Kumar et al. [12] reported that alkalis promoted the earlier

precipitation of portlandite and end of the induction period due to the increase of the pH of the pore solution. In our study, the intensity of the shoulder assigned to portlandite precipitation in the heat flow curve (see Fig. 2) appeared at a shorter time and with an enhanced intensity in  $C_3S$  pastes containing 0.3wt% NaSCN in agreement with Kumar et al. [12]. In contrast, a delay of the onset of the acceleration period was observed in  $C_3S$  pastes with  $Na_2S_2O_3$ , being the delay longer with the increased dosage of this admixture. A similar delay was previously observed in the literature [36] in  $C_3S$  pastes in presence of divalent anions such as  $SO_4^{2-}$  and explained by the electrostatic interactions between the sulfate ions and the  $C_3S$  surface. In particular, Nicoleau et al. [36] argued that the formation of neutral  $CaSO_4^0$  species reduced the charge screening provided by calcium cations, that led to a more negative surface charge and a decrease of the  $C_3S$  dissolution rate. A similar mechanism could be proposed to be responsible of the extension of the induction period induced by another divalent anion such as  $S_2O_3^{2-}$ . Furthermore, the greater slope of the acceleration period in  $C_3S$  pastes containing NaSCN and  $Na_2S_2O_3$  compared to plain pastes, would indicate that both admixtures favoured (1) either the precipitation of a higher number of C–S–H nuclei during the induction period that grow over the acceleration period or (2) the faster growth of C–S–H [37, 38]. However, with the results provided by the current study is not possible to distinguish which mechanism these accelerating admixtures mainly act. Controlled precipitation experiments of C–S–H in presence of

**Fig. 12** Two-dimensional scatter plots of atomic ratio of model cement pastes at 7 days of hydration

admixtures in combination with kinetic analysis, as described in the literature [39, 40], would be required to determine how NaSCN and  $\text{Na}_2\text{S}_2\text{O}_3$  influence the nucleation and growth of C–S–H.

The hydration kinetics and phase assemblage studies done in  $\text{C}_3\text{S}$  and model cement pastes concluded that both alkali salts mainly act on the  $\text{C}_3\text{S}$  phase while not significant impact on the reactivity of the  $\text{C}_3\text{A}$  phase was determined by QXRD (see Fig. 7b). As a consequence, both admixtures led to a higher amount of C–S–H and portlandite with respect to non-admixed pastes. However, while  $\text{Na}_2\text{S}_2\text{O}_3$  and NaSCN enhanced the reactivity of the  $\text{C}_3\text{S}$  pastes over 7 days of hydration compared to non-admixed pastes, they only increased the reactivity of model cement pastes at early ages (up to 14–20 h). In particular, at 7 days of hydration, the addition of 2 wt%  $\text{Na}_2\text{S}_2\text{O}_3$  decreased 12% the cumulative heat and 4% the bounded water. This is in agreement with previous results of Mota et al. [11] who also reported a decrease of the degree of hydration of white cement (calculated from calorimetry tests) in presence of  $\text{Na}_2\text{SO}_4$  and NaOH after 35 h hours although the reason still remains unclear and needs further investigation.

#### b. Influence of NaSCN and $\text{Na}_2\text{S}_2\text{O}_3$ on the C–S–H morphology and microstructure

$\text{Na}_2\text{S}_2\text{O}_3$  and NaSCN both influenced the morphology of C–S–H and microstructure for both,  $\text{C}_3\text{S}$  and the model cement pastes. At a degree of hydration of 9%, the addition of  $\text{Na}_2\text{S}_2\text{O}_3$  to  $\text{C}_3\text{S}$  pastes led to the formation of thicker convergent C–S–H needles and a slightly lower specific surface area than plain pastes, while a greater number of thinner C–S–H needles were formed in  $\text{C}_3\text{S}$ -containing NaSCN with a consequent increase of the  $\text{SSA}_{\text{BET}}$  from 5.4  $\text{m}^2/\text{g}$  in plain samples to 9.8  $\text{m}^2/\text{g}$  in those containing NaSCN. This contrasts with the results obtained by Mota et al. [41], in which divergent C–S–H needles were formed in presence of sulfates in the pore solution and C–S–H with a foil-like structure was formed in alite pastes containing NaOH, however, these authors did not report an impact of the admixtures on the thickness of the C–S–H needles. Further studies on the impact of the changes of the C–S–H morphology, and consequently, the number of contact points, on the mechanical strength are needed.

Both accelerating admixtures increased the Ca/Si of the matrices from 1.72 in the plain  $\text{C}_3\text{S}$ , to 2.27 and

2.09 for  $\text{C}_3\text{S}$  pastes containing  $\text{Na}_2\text{S}_2\text{O}_3$  and NaSCN, respectively (see Table). This higher Ca/Si ratios could be explained by the intermixing of C–S–H with microcrystalline portlandite as the comparison of the calculated and experimental amount water molecules of C–S–H and portlandite, Table 3, concluded that the stoichiometry of C–S–H in non-admixed and admixed pastes had a constant value of  $\text{C}_{1.67}\text{SH}_{2.5}$ . However, both admixtures seemed to influence the distribution of portlandite in  $\text{C}_3\text{S}$  pastes. In general, bigger clusters of portlandite were observed by BSEM in admixed  $\text{C}_3\text{S}$  pastes after 7 days of hydration. Furthermore, the correlation of the portlandite content versus the degree of hydration (see Fig. 5) confirmed that the admixtures did not favour the precipitation of more portlandite overtime. This means that  $\text{Na}_2\text{S}_2\text{O}_3$  and NaSCN changed the portlandite distribution (forming more clusters) but the higher amount of portlandite measured by TGA and XRD was associated with the higher degree of reaction induced by these admixtures.

A greater intermixing of AFm and C–S–H was observed in admixed model cement pastes with respect to the plain samples. While the binary plot concluded the formation of monosulfoaluminate, the QXRD concluded the formation of hemicarboaluminate that would indicate the possible carbonation of the samples during XRD sample preparation and analysis.

Furthermore, the addition of  $\text{Na}_2\text{S}_2\text{O}_3$  and NaSCN increased the amount of outer C–S–H product and a greater porosity as qualitatively observed by BSEM, Figs. 10 and 11.

The studies described above have enabled to gain further knowledge on the influence of  $\text{Na}_2\text{S}_2\text{O}_3$  and NaSCN on the reactivity and microstructure of model Portland cements with  $\text{C}_3\text{S}$  and  $\text{C}_3\text{A}$  as main phases.  $\text{Na}_2\text{S}_2\text{O}_3$  has also been previously reported to enhance the reactivity of synthetic glasses with compositions similar to supplementary cementitious materials (SCMs) [42]. Future studies on the working mechanism and the impact of these alkali salts on the reactivity, phase assemblage and mechanical properties of real blended cements are still required. In particular, the impact of these admixtures on the reactivity of clinker phases and SCMs in blends, their synergistic reactions and its contribution to the formation of hydrates should be investigated. Moreover, the effect of these admixtures on the nucleation and growth of C–S–H needs to be better understood as



well as their influence on the late hydration period. That will enable to design more effective accelerators of the reactivity of the clinker phases and SCMs to further decrease the cement clinker factor without detriment of the early mechanical properties of concrete.

## 5 Conclusions

In this paper, the impact of two accelerating admixtures commonly used, NaSCN and Na<sub>2</sub>S<sub>2</sub>O<sub>3</sub>, on the reactivity and microstructure of pastes of model systems, C<sub>3</sub>S and model cement, was investigated.

The hydration kinetics and phase assemblage studies concluded that both alkali salts mainly acted on the C<sub>3</sub>S phase while not significant impact on the reactivity of the C<sub>3</sub>A phase was measured. As a consequence, a higher amount of C–S–H and portlandite in admixed pastes was measured by QXRD and TGA while not great impact of the admixtures on the amount of the hydrated aluminate phases was determined. Na<sub>2</sub>S<sub>2</sub>O<sub>3</sub> and NaSCN enhanced the reactivity of the C<sub>3</sub>S pastes over 7 days of hydration, while they only increased the reactivity of model cement pastes up to 14–20 h.

The addition of both alkali salts did not modify the C–S–H stoichiometry but they influenced its morphology. At an equal degree of hydration of 9% of C<sub>3</sub>S pastes, thicker convergent C–S–H needles were formed in pastes containing Na<sub>2</sub>S<sub>2</sub>O<sub>3</sub> compared to non-admixed systems, while a greater number of thinner C–S–H needles were formed in presence of NaSCN.

Greater portlandite clusters and greater intermixing of AFm and C–S–H were observed in admixed C<sub>3</sub>S and model cement pastes, respectively, compared to plain systems. Furthermore, admixed samples showed a greater porosity, as qualitatively observed by BSEM, compared to plain cementitious systems.

Further research on the influence of these alkali salts on reaction kinetics, microstructure and macroscopic properties of real blended cements are still needed. This will contribute to develop effective accelerators to further increase clinker replacement in blends without detriment to the early mechanical properties of concrete. Moreover, the impact of Na<sub>2</sub>S<sub>2</sub>O<sub>3</sub> and NaSCN on the C–S–H nucleation and growth should be better understood.

**Acknowledgements** Consejería de Educación e Investigación (Comunidad de Madrid) is thanked for funding the 2016-T1/AMB-1434 project in the frame of “Ayudas de Atracción de Talento Investigador”. Dr. Palacios also thanks CSIC for funding the PIE 2021601023 project. Prof. De la Torre thanks Junta de Andalucía for the P18-RT-720 research project (cofunded by ERDF). The authors also thank Prof. Blanco-Varela (IETcc-CSIC, Spain), Prof. Puertas (IETcc-CSIC, Spain), Prof. Bowen (EPFL, Switzerland) and Prof. Flatt (ETHZ, Switzerland) for their fruitful scientific discussions.

**Funding** Open Access funding provided thanks to the CRUE-CSIC agreement with Springer Nature.

**Open Access** This article is licensed under a Creative Commons Attribution 4.0 International License, which permits use, sharing, adaptation, distribution and reproduction in any medium or format, as long as you give appropriate credit to the original author(s) and the source, provide a link to the Creative Commons licence, and indicate if changes were made. The images or other third party material in this article are included in the article's Creative Commons licence, unless indicated otherwise in a credit line to the material. If material is not included in the article's Creative Commons licence and your intended use is not permitted by statutory regulation or exceeds the permitted use, you will need to obtain permission directly from the copyright holder. To view a copy of this licence, visit <http://creativecommons.org/licenses/by/4.0/>.

## References

- Dorn T, Hirsch T, Stephan D (2021) Analyzing the early structural build-up of accelerated cement pastes. *Mater Struct* 54:67. <https://doi.org/10.1617/s11527-021-01662-5>
- Alahrache S, Winnefeld F, Champenois J-B, Hesselbarth F, Lothenbach B (2016) Chemical activation of hybrid binders based on siliceous fly ash and Portland cement. *Cement Concr Compos* 66:10–23. <https://doi.org/10.1016/j.cemconcomp.2015.11.003>
- Sánchez-Herrero MJ, Fernández-Jiménez A, Palomo Á (2015) Alkaline hydration of C2S and C3S. *J Am Ceram Soc*. <https://doi.org/10.1111/jace.13985>
- Hoang K, Justnes H, Geiker M (2016) Early age strength increase of fly ash blended cement by a ternary hardening accelerating admixture. *Cem Concr Res* 81:59–69. <https://doi.org/10.1016/j.cemconres.2015.11.004>
- Boscaro F, Palacios M, Flatt RJ (2021) Formulation of low clinker blended cements and concrete with enhanced fresh and hardened properties. *Cement Concr Res* 150:106605. <https://doi.org/10.1016/j.cemconres.2021.106605>
- Wang J, Niu D, Zhang Y (2016) Microstructure and mechanical properties of accelerated sprayed concrete. *Mater Struct* 49:1469–1484. <https://doi.org/10.1617/s11527-015-0589-3>
- Peterson VK, Juenger MCG (2006) Hydration of tricalcium silicate: effects of CaCl<sub>2</sub> and sucrose on reaction kinetics



- and product formation. *Chem Mater* 18:5798–5804. <https://doi.org/10.1021/cm061724y>
8. Riding K, Silva DA, Scrivener K (2010) Early age strength enhancement of blended cement systems by  $\text{CaCl}_2$  and diethanol-isopropanolamine. *Cem Concr Res* 40:935–946. <https://doi.org/10.1016/j.cemconres.2010.01.008>
  9. Juenger MCG, Monteiro PJM, Gartner EM, Denbeaux GP (2005) A soft X-ray microscope investigation into the effects of calcium chloride on tricalcium silicate hydration. *Cem Concr Res* 35:19–25. <https://doi.org/10.1016/j.cemconres.2004.05.016>
  10. Jawed I, Skalny J (1978) Alkalies in cement: a review: II. Effects of alkalies on hydration and performance of Portland cement. *Cem Concr Res* 8:37–51. [https://doi.org/10.1016/0008-8846\(78\)90056-X](https://doi.org/10.1016/0008-8846(78)90056-X)
  11. Mota B, Matschei T, Scrivener K (2018) Impact of  $\text{NaOH}$  and  $\text{Na}_2\text{SO}_4$  on the kinetics and microstructural development of white cement hydration. *Cem Concr Res* 108:172–185. <https://doi.org/10.1016/j.cemconres.2018.03.017>
  12. Kumar A, Sant G, Patapy C, Gianocca C, Scrivener KL (2012) The influence of sodium and potassium hydroxide on alite hydration: experiments and simulations. *Cem Concr Res* 42:1513–1523. <https://doi.org/10.1016/j.cemconres.2012.07.003>
  13. Abdelrazig BEI, Bonner DG, Nowell DV, Dransfield JM, Egan PJ (1990) Effects of accelerating admixtures on cement hydration. In: *En admixtures for concrete-improvement of properties*. CRC Press
  14. Wise T, Ramachandran VS, Polomark GM (1995) The effect of thiocyanates on the hydration of portland cement at low temperatures. *Thermochim Acta* 264:157–171. [https://doi.org/10.1016/0040-6031\(95\)02323-T](https://doi.org/10.1016/0040-6031(95)02323-T)
  15. Murakami K, Tanaka H, Komatsu T (1968) The accelerating action of calcium thiosulfate on the hydration of Portland cement and comparison with other inorganic salts. *J Ceram Assoc Jpn* 76:373–384. [https://doi.org/10.2109/jcersj1950.76.879\\_373](https://doi.org/10.2109/jcersj1950.76.879_373)
  16. Marchon D (2016) Controlling cement hydration through the molecular structure of comb copolymer superplasticizers. [http://e-collection.library.ethz.ch/view/eth:50178?q=\(author:Marchon\)](http://e-collection.library.ethz.ch/view/eth:50178?q=(author:Marchon)). Accessed Jan 19, 2017.
  17. Palacios M, Kazemi-Kamyab H, Mantellato S, Bowen P (2016) Chapter 10. Laser diffraction and gas adsorption techniques. In: *A practical guide to microstructural analysis of cementitious materials*. CRC Press. Taylor and Francis Group
  18. Hewlett PC, Liška M (1998) *Lea's chemistry of cement and concrete*, 4th edn. Butterworth-Heinemann, Oxford
  19. Pustovgar E, Sangodkar RP, Andreev AS, Palacios M, Chmelka BF, Flatt RJ, d'Espinose de Lacaillerie J-B (2016) Understanding silicate hydration from quantitative analyses of hydrating tricalcium silicates. *Nat Commun* 7:10952. <https://doi.org/10.1038/ncomms10952>
  20. Linderöth O, Wadsö L, Jansen D (2021) Long-term cement hydration studies with isothermal calorimetry. *Cem Concr Res* 141:106344. <https://doi.org/10.1016/j.cemconres.2020.106344>
  21. Marchon D, Juilland P, Gallucci E, Frunz L, Flatt RJ (2017) Molecular and submolecular scale effects of combopolymers on tri-calcium silicate reactivity: toward molecular design. *J Am Ceram Soc* 100:817–841. <https://doi.org/10.1111/jace.14695>
  22. De La Torre AG, Bruque S, Aranda MAG (2001) Rietveld quantitative amorphous content analysis. *J Appl Cryst* 34:196–202. <https://doi.org/10.1107/S0021889801002485>
  23. Brindley GW (1945) The effect of grain or particle Size on x-ray reflections from mixed powders and alloys, considered in relation to the quantitative determination of crystalline substances by x-ray methods. *London Edinburgh Dublin Philos Mag J Sci* 36:347–369. <https://doi.org/10.1080/14786444508520918>
  24. Lothenbach B, Durdziński PT, De Weerd K (2016) Chapter 5. Thermogravimetric analysis. In: Scrivener K, Snellings R, Lothenbach B (eds) *A practical guide to microstructural analysis of cementitious materials*. CRC Press, Taylor and Francis Group, New York
  25. Zea-Garcia JD, De la Torre AG, Aranda MAG, Santacruz I (2020) Processing and characterisation of standard and doped alite-belite-ye'elite ecocement pastes and mortars. *Cem Concr Res* 127:105911. <https://doi.org/10.1016/j.cemconres.2019.105911>
  26. Mantellato S, Palacios M, Flatt RJ (2016) Impact of sample preparation on the specific surface area of synthetic ettringite. *Cem Concr Res* 86:20–28. <https://doi.org/10.1016/j.cemconres.2016.04.005>
  27. Pustovgar E, Mishra RK, Palacios M, d'Espinose de Lacaillerie J-B, Matschei T, Andreev AS, Heinz H, Verel R, Flatt RJ (2017) Influence of aluminates on the hydration kinetics of tricalcium silicate. *Cem Concr Res* 100:245–262. <https://doi.org/10.1016/j.cemconres.2017.06.006>
  28. Wagner D, Bellmann F, Neubauer J (2020) Influence of aluminium on the hydration of triclinc C3S with addition of KOH solution. *Cem Concr Res* 137:106198. <https://doi.org/10.1016/j.cemconres.2020.106198>
  29. Andrade Neto JS, Rodríguez ED, Monteiro PJM, De la Torre AG, Kirchheim AP (2022) Hydration of C3S and Al-doped C3S in the presence of gypsum. *Cem Concr Res* 152:106686. <https://doi.org/10.1016/j.cemconres.2021.106686>
  30. Snellings R, Salze A, Scrivener KL (2014) Use of X-ray diffraction to quantify amorphous supplementary cementitious materials in anhydrous and hydrated blended cements. *Cem Concr Res* 64:89–98. <https://doi.org/10.1016/j.cemconres.2014.06.011>
  31. Garbev K, Bornefeld M, Beuchle G, Stemmermann P (2008) Cell dimensions and composition of nanocrystalline calcium silicate hydrate solid solutions. Part 2: X-ray and thermogravimetry study. *J Am Ceram Soc* 91:3015–3023. <https://doi.org/10.1111/j.1551-2916.2008.02601.x>
  32. Cuesta A, Zea-Garcia JD, Londono-Zuluaga D, De la Torre AG, Santacruz I, Vallcorba O, Dapiaggi M, Sanfeliú SG, Aranda MAG (2018) Multiscale understanding of tricalcium silicate hydration reactions. *Sci Rep* 8:8544. <https://doi.org/10.1038/s41598-018-26943-y>
  33. Sun GK, Young JF, Kirkpatrick RJ (2006) The role of Al in C–S–H: NMR, XRD, and compositional results for precipitated samples. *Cem Concr Res* 36:18–29. <https://doi.org/10.1016/j.cemconres.2005.03.002>
  34. Rossen JE (2014) Composition and morphology of C–A–S–H in pastes of alite and cement blended with supplementary



- cementitious materials. EPFL. <https://doi.org/10.5075/epfl-thesis-6294>
35. Scrivener K, Bazzoni A, Mota B, Rossen JE (2016) Electron microscopy. In: A practical guide to microstructural analysis of cementitious materials. CRC Press
  36. Nicoleau L, Schreiner E, Nonat A (2014) Ion-specific effects influencing the dissolution of tricalcium silicate. *Cem Concr Res* 59:118–138. <https://doi.org/10.1016/j.cemconres.2014.02.006>
  37. Scrivener KL, Juilland P, Monteiro PJM (2015) Advances in understanding hydration of Portland cement. *Cem Concr Res* 78(Part A):38–56. <https://doi.org/10.1016/j.cemconres.2015.05.025>
  38. Scherer GW, Bellmann F (2018) Kinetic analysis of C–S–H growth on calcite. *Cem Concr Res* 103:226–235. <https://doi.org/10.1016/j.cemconres.2016.07.017>
  39. Andalibi MR, Kumar A, Srinivasan B, Bowen P, Scrivener K, Ludwig C, Testino A (2018) On the mesoscale mechanism of synthetic calcium–silicate–hydrate precipitation: a population balance modeling approach. *J Mater Chem A* 6:363–373. <https://doi.org/10.1039/C7TA08784E>
  40. Harris M, Simpson G, Scrivener K, Bowen P (2022) A method for the reliable and reproducible precipitation of phase pure high Ca/Si ratio (>1.5) synthetic calcium silicate hydrates (CSH). *Cem Concr Res* 151:106623. <https://doi.org/10.1016/j.cemconres.2021.106623>
  41. Mota B, Matschei T, Scrivener K (2015) The influence of sodium salts and gypsum on alite hydration. *Cem Concr Res* 75:53–65. <https://doi.org/10.1016/j.cemconres.2015.04.015>
  42. Gonzalez-Panicello L, Garcia-Lodeiro I, Puertas F, Palacios M (2022) Influence of accelerating admixtures on the reactivity of synthetic aluminosilicate glasses. *Materials* 15:818. <https://doi.org/10.3390/ma15030818>
- Publisher's Note** Springer Nature remains neutral with regard to jurisdictional claims in published maps and institutional affiliations.

